RSC Advances

ROYAL SOCIETY OF CHEMISTRY

www.rsc.org/advances

RSC Advances

RSCPublishing

ARTICLE

Anchoring Nano-Sulfur on Flat Graphene as Cathode Material for Lithium-Sulfur Battery

Cite this: DOI: 10.1039/x0xx00000x

Bin Li, Songmei Li*, Jianhua Liu, Jingjing Xu

Received 00th January 2012,
Accepted 00th January 2012

DOI: 10.1039/x0xx00000x

www.rsc.org/

Nano-Sulfur anchored on flat graphene (Nano-S/FG) was achieved by a facile hydrothermal method as high performance cathode materials for lithium-Sulfur battery. The obtained Nano-S/FG shows flat morphologies dispersed with numerous nano-size sulfur particles. Remarkably, nanocrystalline sulfur was anchored on the surfaces of graphene with the help of S-O bond. The resulted Nano-S/FG with sulfur content as high as 75.4% exhibited excellent lithium storage performance with a high specific reversible capacity of 1268mAhg^{-1} at the current of 200mA g^{-1}, and a specific reversible capacity of 536mAhg^{-1} even at the high current of 3200mAg^{-1}. Additionally, the reversible capacity can retain as high as 900mAh g^{-1} after 200cycles. It can be believed that this work supplied a considerable choice for lithium-sulfur battery.

1. Introduction

There is no doubt that the demand for clean and efficient energy storage devices is becoming more and more critical for future markets, such as plug-in hybrid vehicle and electric vehicle technologies.[1] Lithium battery system is one of the most promising candidates owing to their high specific energy and power density.[2] However, the commercialized lithium ion batteries will become insufficient for the future electronic devices due to the low capacity of conventional cathode materials (for example, ~150 mAh g^{-1} for layered oxides and ~170 mAh g^{-1} for $LiFePO_4$)[3].Developing novel electrode materials with higher gravimetric and volumetric capacities is becoming increasingly urgent. Sulfur, as one of the most abundant elements on the earth, can react with metallic lithium to form Li_2S by a two-electron reaction, and offers a high theoretical capacity of 1675 mAh g^{-1} and a high theoretical energy density of 2600 Wh kg^{-1}, making it a potential high capacity cathode material for the next rechargeable batteries.[4-7]

Although the Li-S battery is believed to be one of the most promising next-generation high-energy-density rechargeable batteries, the cycle life and efficiency need to be improved when employed in practical applications. The sulfur cathode suffers two principle problems: shuttle effect of polysulfides and insulate of sulfur cathode. To drive shuttle effect, physical methods (Polymer-coated, Porous package and so on)[8-11], chemical methods (hydroxyl bond and sulfur-carbon bond)[12-14] and composite methods were also induced.[9, 14] To improve the insulation of sulfur cathode, various kinds of conductive material were employed such as mesoporous carbon, acetylene black, carbon fiber, polypyrrole, polyaniline and graphene. Some are introduced to solve the both problems.[2, 15-18]

Among these materials, graphene (or graphene oxide) was a remarkable choice due to its unique two-dimensional structure and excellent electrical properties.[8, 11, 13, 16, 19, 20] Graphene (or graphene oxide) was employed for compositing sulfur/graphene for Li-S battery in many recent report. Y. Cui et.al used Graphene oxide sheets to wrap sulfur particles[8], obtained sulfur-graphene composites with high capacity and cycling stability. The resulting graphene-sulfur composite showed high and stable specific capacities up to ~600 mAh/g over more than 100 cycles. Arumugam Manthiram et.al prepared hydroxylated graphene-sulfur nanocomposites with the aid of ultrasonication,[21] and the resulting graphene-sulfur composite showed high rate performance. These works show utilizes of the physical or chemical property of graphene oxide. However the sulfur particles were coating or enwrapping in graphene, which induce difficult Li^+ ions conduct.

In order to develop efficient sulfur composites materials, herein, a new structure Sulfur-Graphene composite was synthesized by hydrothermal methods. Nano-Sulfur/Flat Graphene (denoted as Nano-S/FG) was synthesized. Graphene oxide sheets and $Na_2S_2O_3$ were used as graphene and sulfur resource by in situ reaction. Cationic surfactant (CTAB) was added to control flexible graphene to flat morphology.[22] The obtained Nano-S/FG composite shows a unique flat morphology of graphene sheets with nano-size sulfur anchored on it. The electrode with Nano-S/FG as cathode exhibited

*Key Laboratory of Aerospace Advanced Materials and Performance of Ministry of Education, School of Materials Science and Engineering, Beihang University, Beijing, 100191, China. E-mail: songmei_li@buaa.edu.cn; Fax: +86-10-82317103; Tel: +86-10-82317103

† Electronic supplementary information (ESI) available. See DOI:

high capacity and long-cycle retention (1268mAhg^{-1} at the first charge and 900 mAhg^{-1} at the 200th charge).

2. Experimental

2.1 Preparation of Nano-S/FG

The Graphene Oxide sheets (GOs) were prepared by modified Hummers' method. The nano-sulfur anchored on flat graphene composite was prepared by hydrothermal methods with cationic surfactant cetyltrimethylammonium bromide (CTAB).Three steps should be concluded in the prepare process: Firstly, 0.5 wt.% CTAB and a certain amount of $Na_2S_2O_3$ was added in 5mg/mL GOs suspension under stirring. Secondly, chlorhydric acid was added dropwise under stirring until gas drained, element sulfur generated as the following reaction.

$Na_2S_2O_3+2HCl \rightarrow 2NaCl+H_2O+SO_2+S\downarrow$

Thirdly, the mixed solution was transferred to Teflon-lined stainless steel autoclave sealed tightly and heated at a temperature of 160℃ in a preheated electric oven for 2h. After that the autoclave was allowed to cool to room temperature and the precipitates were a hydrogels sulfur-graphene. The hydrogels were washed several times with deionized water to removed remaining impurity and then freeze-drying to obtain hydrogels as showed in Scheme 1. As a comparison, a common S/G composite was synthesized as the same route without cationic surfactant.

2.2 Material characterization

The morphologies were examined by scanning electron microscopy (SEM, JEOL-7500), and transmission electron microscopy (TEM, JEM 2100F). Powder X-ray diffraction (XRD, CuKa radiation, Bruker D8) was used to verify the component of the composite. The sulfur content in the S/G was ascertained by the thermogravimetric/differential thermal analysis (TG/DTA) measurement (Netzsch STA 449C thermal analyzer). Raman spectra were obtained from a RENISHAW spectrometer (inVia Reflex) to investigate the characteristics of the reducing degree of graphene oxide A He-Ne laser operating at λ=632.8nm was used as the excitation source.X-ray photoelectron spectra (XPS) were employed to character element sulfur and carbon, which performed on an ESCALAB 250Xi Spectrometer (Thermo Scientific).

2.3. Electrochemical measurement

The electrodes were prepared by dispersing the as-prepared composites (80 wt%), acetylene carbon black (10 wt%) and poly(-vinylidene fluoride) binder (10 wt%) in N-methyl-2-pyrrolidone solvent to form a slurry. The slurry was pasted onto steel foil current collector and dried at 60℃ for 12 h in a vacuum oven. The electrochemical measurements were carried out by two-electrode coin cells with a lithium foil as the counter electrode. The CR2025-type coin cells were assembled in an aFGn-filled glove box. The electrolyte solution was 1 M LiTFSI in a solvent of DOL:DME (1:1 in volume). An electrochemistry workstation (Shanghai Chenhua Instruments Co. Ltd.) was employed for cyclic voltammetry (CV) and electrochemical impedance spectrometry (EIS). CV was carried out in the voltage range of 1.2-3.0 V with a constant scan rate of 0.5 mV s^{-1} and EIS was carried out in the frequency from 10^5Hz to 10^{-2}Hz with 5mV amplitude. The galvanostatic charge and discharge measurements were conducted on an ARBIN BT2000 battery test system at different current densities in the voltage range from 1.5 to 3.0 V. The mass loading of the composites was about 2mg/cm^2. The cell capacity was calculated based on the weight of sulfur.

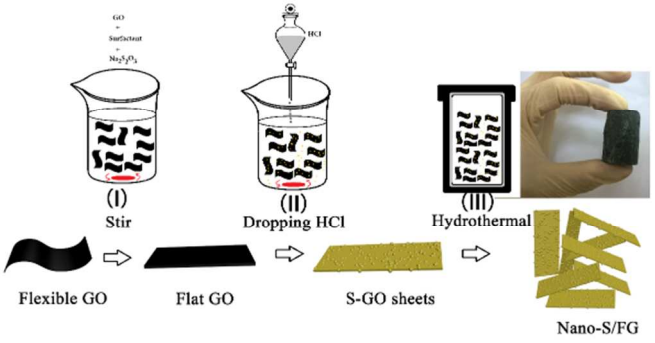

Scheme 1. Nano-S/FG Fabrication process.

3. Results and discussion

Fig. 1 shows a schematic representation of the preparation of Nano-S/FG through hydrothermal method. Typically, three steps were included in the preparation process: (I) CTAB and $Na_2S_2O_3$ was added in GO suspension to control flexible graphene to flat (fGO); (II) HCl was added by dropwise to produce sulfur on graphene oxide in situ; (III) hydrothermal process to form nano-S/FG composite. Notably, the sulfur content in the composites was controlled by the amount of $Na_2S_2O_3$. As compared, common S/G composites was prepared by the same methods except without CTAB (denoted as S/G).

XRD patterns of S/G, Nano-S/FG and pure S were shown in Fig.1a. Both the Nano-S/FG and S/G had different diffraction peaks with the crystalline sulfur which indicated that the sulfur have different crystal structure. However there are many small diffraction peaks at the position of the typical sulfur crystal diffraction peaks position indicating that smaller crystal sulfur existed in the composite. Then, sulfur content was confirmed by TGA (as shown in fig.1b), the sulfur mass percent of Nano-S/FG was 75.4 wt.% which is almost the same as the theory content. Additionally, the mass loss temperature at above 200°C indicated that element sulfur was synthesis successfully by our methods. Meanwhile, the high sulfur evaporation temperature (above 200°C) indicated the strong binding force between sulfur and FG host.

The structure and morphology of Nano-S/FG were firstly characterized by SEM and TEM. From Fig.2a, it is clearly seen that the graphene was flat and random distributed, which was different from the S/G prepared without CTAB (Fig.S1). It should be noted that sulfur particles are invisible from the SEM image in Fig. 2a and 2b, while there are many sulfur particles in the S-GO sheets without

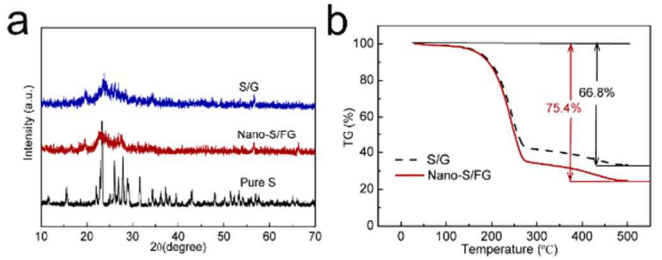

Fig.1 (a) XRD patterns of pure sulfur, Nano-S/FG and S/G; (b) TG curve of S/G and Nano-S/FG.

hydrothermal process (Fig.S2), which indicated that the nano-size sulfur was formed in the hydrothermal process. And then EDS mapping was employed to character the distribution of sulfur and carbon. As exhibited in the inset image of Fig.2b, the element sulfur and carbon was uniform dispersed in the composites, which is important for the sulfur-carbon composites for lithium-sulfur battery according to the literatures.[9, 12, 13, 15] In order to further obverse dispersion of the sulfur, TEM and HRTEM were employed. TEM image revealed that there are numerous sulfur particles dispersed on the surface of graphene (Fig.2c). Meanwhile, the HRTEM image (as shown in Fig.2d) illustrated that the size of nano-sulfur was about 5nm, which is different with the common sulfur particle.

Raman spectra was employed to confirm that the graphene oxide has been reduced in hydrothermal process. As shown in Fig.3a, there are two peaks at 1350 and 1580cm^{-1} in the Raman spectrum of S-GO and Nano-S/FG, which should be assigned to the D band and G band of graphene since both of them are present in the Raman spectrum of graphene oxide.[11, 14] However, the ratios of D and G bands of Nano-S/FG is estimated to be greater than 2, which is significantly greater than that of S-GO (about 1.3) indicating graphene oxide was partially reduced during our hydrothermal process. And then FTIR was used to confirm that the Nano-S was

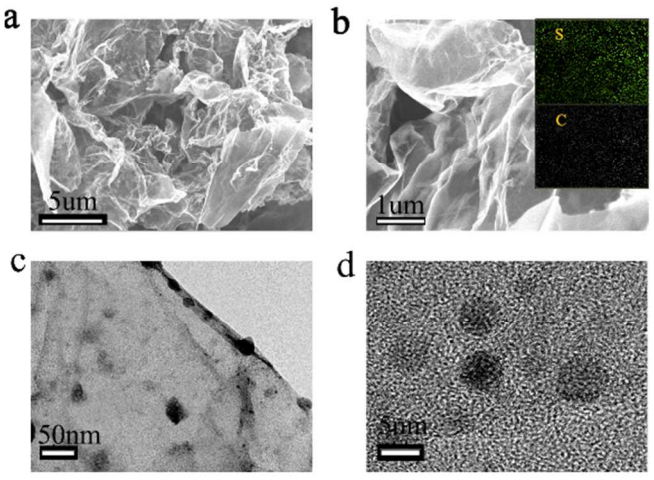

Fig.2 Morphology of Nano-S/FG. (a) SEM image, (b) EDS mapping, (c) TEM image, (d) HRTEM image.

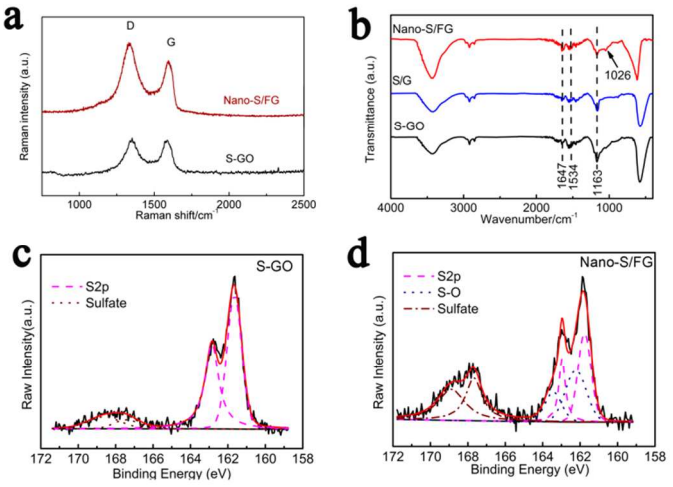

Fig.3 Structure characterize of Nano-S/FG and S-GO. (a) Raman spectrometry, (b) FT-IR spectrometry, (c, d) S2p high resolution spectrum of S-GO and Nano-S/FG.

anchored on graphene, as shown in Fig.3b. There are three peaks on S-GO and S/G located at 1163, 1534 and 1647cm^{-1}, which are assigned to stretching vibrations of C-O, S=O and C=O respectively.[12, 13, 21] The intensity of these peaks on S/G was weaken than that of S-GO, which indicated the hydro hydrothermal process reduce of graphene oxide. It should be noted that there is a new peak appeared at 1026cm^{-1} on spectrum of Nano-S/FG, which is due to the stretching vibrations of S-O. The S-O bond was appeared after hydrothermal process with the help of CTAB and the S-O bond is help for immobilizing polysulfide during the charge-discharge process.

To further understand the anchor bond between graphene host and sulfur, the S2p high resolution spectrum of S-GO and Nano-S/FG were detected by XPS and illustrated in Fig.3c, 3d respectively. From Fig.3c, it was found most of element sulfur was existed as S2p and a little of sulfate, which meant the production of step II is elemental sulfur. However after hydrothermal treatment, it should be seen that the sulfate banding intensity is increasing obvious, which indicated there oxide of sulfur in the hydrothermal process. More important, there is a lot of S-O banding appeared in Fig 3d, which is the anchor bonding between graphene host and sulfur, and these results is consistent with the FTIR results. Additionally, C1s spectrum was employ to prove the reducing process and the anchor bond and shown in Fig. S3. As shown in Fig.S3, the intensity of O-C=O and C=O in Nano-S/FG is significantly dropped when compared with that in S-GO, which further proved the graphene oxide was reduced.[11-13, 21, 23] However, the C-O bonding intensity isn't decrease in the hydrothermal process, which might be due to the C-O-S bonding generate. These discuss the S-O bonding was generated in the hydrothermal process, which is favourable for the stability of polysulfide during cycle process as they are used as cathode materials for lithium-sulfur batteries.

Electrochemical properties of the Nano-S/FG composite as cathode for lithium-sulfur battery are presented in Fig.4. Fig. 4a displays the typical cyclic voltammetry (CV) curves of lithium sulfur

batteries with Nano-S/FG cathodes in the voltage range of 1.2-3.0 V with a constant scan rate of 0.5 mV s^{-1}. One oxidation peak and two distinct reduction peaks can be observed. The oxidation peak at the potential of 2.5 V is corresponding to the conversion of lithium sulfide into high-order polysulfide.[24] Two pronounced reduction peaks at around 2.0 V and 2.3 V indicated the two-step conversion of elemental sulfur to lithium sulfide respectively.[23] The peak at around 2.3 V associates with the conversion of elemental sulfur to soluble lithium polysulfide (Li_2S_n, $4 \leqslant n \leqslant 8$), and the peak at about 2.0 V is related to the reduction of lithium polysulfide to insoluble Li_2S_2 and Li_2S. In addition, the peak current didn't have obvious change indicating that the Nano-S/FG composite cathode exhibited/possessed good electrochemical stability.

The capacity and cycle performance of Nano-S/FG were evaluated by galvanostatic discharge-charge measurements at a current density of 200mA g^{-1} between 1.4 V and 2.8 V vs. Li/Li^+ (Fig. 4b). From the potential profiles of Nano-S/FG, it is striking to note that capacity of Nano-S/FG was about 1268mAh g^{-1} at the first discharge and have a slight decrease to 1164mAhg^{-1} at the 5th cycle. There are two typical plateaus at the discharge process and one plateau at the discharge process which is consisted with the peak potential of the CV curves. However, the ratio of first plateau with second plateau in discharge stage have a clearly distinguish between first and the subsequent discharge process. This should be due to the high content anchor bonding between sulfur and graphene sheets, which induce activation process the first discharge, and this phenomenon is common in many liquid phase synthesis sulfur-graphene composites according to the literature reports[13,14] . Fig.5c shows the long cycle performance of Nano-S/FG and S/G electrodes at a current density of 200 mAg^{-1}., The initial capacity was about 1268mAhg^{-1} for the Nano-S/FG electrode, and which is higher than

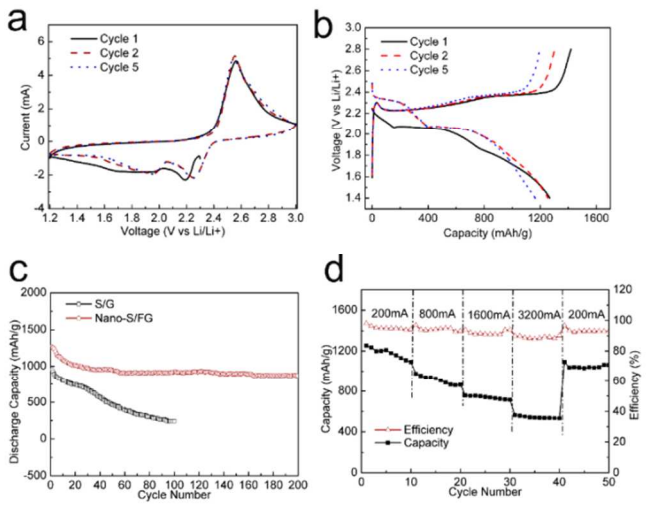

Fig.4 Electrochemical performance of Nano-S/FG as cathode for Lithium-Sulfur battery. (a) Typical cyclic voltammetry curves of Nano-S/FG cathodes, (b) Selected charge-discharge voltage profiles of Nano-S/FG at a current of 200mA g^{-1}. (c) Cycle and capacity of Nano-S/FG and S/G electrode at a current of 200mA g^{-1}. (d) Rate performance of Nano-S/FG.

that of the S/G electrode (1000mAhg^{-1}).The capacity of Nano-S/FG electrode has a slight decrease to 950mAhg^{-1}at the initial 25 cycles and then stabled as high as 900mAhg^{-1} after 200 cycles at a current density of 200mA g^{-1}.These results indicated that the designed Nano-S/FG have a high capacity performance and long cycle performance. Meanwhile, the Nano-S/FG also exhibited good rate performance, which was investigated by increasing the current density from 200mA g^{-1} to 3200mA g^{-1} progressively. The capacity of Nano-S/FG as cathode at a high current density (800mA g^{-1}) is still stable at 736mAh g^{-1}. Even at the highest current density of 3200mAh g^{-1}, the capacity can still be delivered as high as 536mAh g^{-1}. These results suggested that the Nano-S/FG exhibited a good electrochemical performance, which is superior to those reported previously in the literatures through a rough comparison.

In order to understand why the Nano-S/FG electrode possesses excellent electrochemical performances, AC impedance measurements were performed after 50 cycles, and the Nyquist plots was showed in Fig.5a. Generally, the relaxation in the high frequency region is attributed to the ohmic resistance of electrode and electrolyte, and the semicircle in the medium-frequency range is attributed to the Li^+ charge-transfer impedance on the electrode-electrolyte interface. The Nyquist plots showed that the diameter of semicircle for Nano-S/FG in the medium-frequency range is only one fourth as that of S/G. The kinetic differences of Nano-S/FG and S/G electrodes were further investigated by modeling AC impendence spectra based on the equivalent circuit in inset of Fig.5.[25, 26] Among the fitting results (table S1), R_2 are assigned as charge-transfer resistance, which generally represents the transmission performance of the electrode. The R_2 value of Nano-S/FG (76.7 Ω) is only a quarter of that of S/G (269.1 Ω), indicating that the flat graphene improved the conductivity of electrode significantly, even after 50 cycles.

Furthermore, the electrochemical reaction kinetics of Li^+ insertion/deinsertion was studied by CV curve as shown in Fig.6. It can be seen obviously that the anodic peaks shift to low potential and

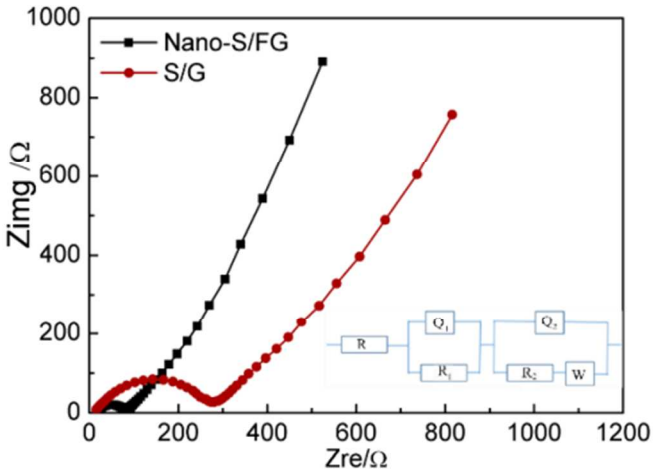

Fig. 5 Nyquist plots of Nano-S/FG and S/G as cathode after 50 charges.

the cathodic peaks shift to high potential with increasing scan rate, and the cathodic peak current (I_{pc}) and anode peak currents (I_{pa}) also increase with increasing scan rate. In addition, all the peak currents of the Nano-S/FG electrode are higher than those of the S/G at each scan rate. The relation between peak currents and scan rates can indicate the electrochemical reaction characteristics.[27-29] For the diffusion-limited process, the peak current is proportional to the square roots of the scan rate ($v^{1/2}$) as the followed equation:

$$I_p=0.4463n^{3/2}F^{3/2}\,C_{Li}SR^{-1/2}T^{1/2}D_{Li}^{1/2}v^{1/2}(25^{o}\,C)$$

Where I_p is the peak current (A), n is the number of electrons per reaction species (for Li ion), F is the Faraday constant (96485C mol^{-1}), C_{li} is the molar concentration of Li^+ (mol cm^{-3}), S is the surface area of the electrode (cm^2), R is the gas constant (8.314J mol^{-1} K^{-1}), T is the absolute temperature (K), D_{Li} is the chemical diffusion coefficient (cm^2 s^{-1})measured by CV, and the v is the scanning rate (V s^{-1}). In this equation, the peak current is in direct proportion to the square root of the scanning rate, which agrees with our results (as showed in Fig.6c and 6d). The slope of the fitted line is dependent of the diffusion coefficient in the equation. Therefore, it can be deduced that the Nano-S/FG had a higher diffusion coefficient in comparison of the slope, indicating that lithium diffusion in Nano-S/FG is more facile. These results demonstrate that the nano sulfur anchored on flat graphene is responsible for its high Li-ion diffusion rate.

Based on the above experimental results, it can be proved that the electrochemical performance of Nano-S/FG electrode is significantly improved by comparison with S/G electrode. The good lithium storage performance of Nano-S/FG cathode can be ascribed to reasons as following: Firstly, the unique flat graphene supplies excellent electrical conductivity and ion conductivity. Secondly, nanocrystalline sulfur synthesized in our proposal provides high reversible capacity for lithium storage. Finally, the nanocrystalline sulfur anchored on the surface of graphene can keep long-term contact with graphene and preserves long cycle performance.

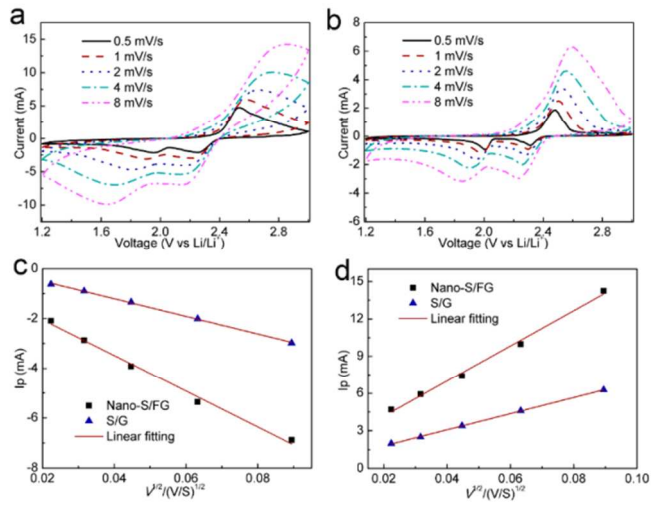

Fig.6 CV plots of the (a) Nano-S/FG and (b) S/G electrode at different scan rates between 1.2V and 3.0V (vs. Li^+/Li) at room temperature and (c) I_{pc} and (d) I_{pa} vs $v^{1/2}$ plots and the corresponding linear fitting.

Conclusions

In summary, we prepared Nano sulfur particles anchored on flat graphene with high sulfur content through a facile hydrothermal method. The obtained Nano-S/FG composite shows a unique morphology of nano-size sulfur anchored on flat graphene sheets. The electrode with Nano-S/FG as cathode exhibited high specific reversible capacity of 1268mAh g^{-1} at the first charge, and stabled about 900 mAh g^{-1} after 200 cycles. Such excellent electrochemical performance indicates that the Nano-S/FG composite is a promising material for application in lithium sulfur batteries.

Acknowledgements

This work was supported by the National Natural Science Foundation of China (51271012).

References:

1. Q. Zhang, E. Uchaker, S. L. Candelaria and G. Cao, *Chem Soc Rev*. 2013, 42, 3127-3171.
2. Y. Yang, G. Zheng and Y. Cui, *Chem Soc Rev*, 2013, **42**, 3018.
3. C. Ban, W. Yin, H. Tang, S. Wei, Y. Yan and A. C. Dillon, *Advanced Energy Materials*, 2012, **2**, 1028-1032.
4. S. Evers and L. F. Nazar, *Accounts Chem Res*, 2012, **46**, 1135-1143.
5. Y. Yin, S. Xin, Y. Guo and L. Wan, *Angewandte Chemie International Edition*, 2013, **52**, 13186-13200.
6. J. Schuster, G. He, B. Mandlmeier, T. Yim, K. T. Lee, T. Bein and L. F. Nazar, *Angewandte Chemie International Edition*, 2012, **51**, 3591-3595.
7. N. Jayaprakash, J. Shen, S. S. Moganty, A. Corona and L. A. Archer, *Angewandte Chemie International Edition*, 2011, **50**, 5904-5908.
8. H. Wang, Y. Yang, Y. Liang, J. T. Robinson, Y. Li, A. Jackson, Y. Cui and H. Dai, *Nano Lett*, 2011, **11**, 2644-2647.
9. W. Bao, Z. Zhang, C. Zhou, Y. Lai and J. Li, *J Power Sources*, 2014, **248**, 570-576.
10. Y. Su and A. Manthiram, *Chem Commun*, 2012, **48**, 8817-8819.
11. S. Evers and L. F. Nazar, *Chem Commun*, 2012, **48**, 1233-1235.
12. R. Demir-Cakan, M. Morcrette, F. Nouar, C. Davoisne, T. Devic, D. Gonbeau, R. Dominko, C. Serre, G. Férey and J. Tarascon, *J Am Chem Soc*, 2011, **133**, 16154-16160.
13. L. Ji, M. Rao, H. Zheng, L. Zhang, Y. Li, W. Duan, J. Guo, E. J. Cairns and Y. Zhang, *J Am Chem Soc*, 2011, **133**, 18522-18525.
14. C. Zhang, W. Lv, W. Zhang, X. Zheng, M. Wu, W. Wei, Y. Tao, Z. Li and Q. Yang, *Advanced Energy Materials*, 2014, **4**, n/a-n/a.
15. J. Guo, Y. Xu and C. Wang, *Nano Lett*, 2011, **11**, 4288-4294.
16. L. Wang, X. He, J. Li, J. Gao, M. Fang, G. Tian, J. Wang and S. Fan, *J Power Sources*, 2013, **239**, 623-627.
17. T. Lin, Y. Tang, Y. Wang, H. Bi, Z. Liu, F. Huang, X. Xie and M. Jiang, *Energy & Environmental Science*, 2013, **6**, 1283-1290.
18. M. Park, J. Yu, K. J. Kim, G. Jeong, J. Kim, T. Yim, Y. Jo, U. Hwang, S. Kang, T. Woo, C. H. Kim and A. Y. Kim, *RSC Advances*, 2013, **3**, 11774.
19. C. Xu, B. Xu, Y. Gu, Z. Xiong, J. Sun and X. S. Zhao, *Energy & Environmental Science*, 2013, **6**, 1388-1414.
20. M. Xiao, M. Huang, S. Zeng, D. Han, S. Wang, L. Sun and Y. Meng, *RSC Advances*, 2013, **3**, 4914-4916.
21. C. Zu and A. Manthiram, *Advanced Energy Materials*, 2013, **3**, 1008-1012.

22. S. Yang, X. Feng, L. Wang, K. Tang, J. Maier and K. Müllen, *Angewandte Chemie International Edition*, 2010, **49**, 4795-4799.
23. J. Jin, Z. Wen, G. Ma, Y. Lu, Y. Cui, M. Wu, X. Liang and X. Wu, *RSC Advances*, 2013, **3**, 2558.
24. K. Xi, S. Cao, X. Peng, C. Ducati, R. Vasant Kumar and A. K. Cheetham, *Chem Commun*, 2013, **49**, 2192-2194.
25. S. Li, B. Wang, J. Liu and M. Yu, *Electrochim Acta*, 2014, **129**, 33-39.
26. S. Yang, X. Feng, L. Zhi, Q. Cao, J. Maier and K. Müllen, *Adv Mater*, 2010, **22**, 838-842.
27. B. Wang, S. Li, J. Liu, M. Yu, B. Li and X. Wu, *Electrochim Acta*, 2014, **146**, 679-687.
28. K. Tang, X. Yu, J. Sun, H. Li and X. Huang, *Electrochim Acta*, 2011, **56**, 4869-4875.
29. Y. Shi, L. Wen, F. Li and H. Cheng, *J Power Sources*, 2011, **196**, 8610-8617.